ARL-TR-10244 ● Dec 2025

DEVCOM ARMY RESEARCH LABORATORY

Modeling the Thermal History–Microstructure Links in Equal Channel Angular Extrusion

by Philip E. Goins and Kristopher A. Darling

NOTICES

Disclaimers

The findings in this report are not to be construed as an official Department of the Army position unless so designated by other authorized documents.

Citation of manufacturer's or trade names does not constitute an official endorsement or approval of the use thereof.

Destroy this report when it is no longer needed. Do not return it to the originator.

ARL-TR-10244 ● DEC 2025

Modeling the Thermal History–Microstructure Links in Equal Channel Angular Extrusion

Philip E. Goins and Kristopher A. Darling
DEVCOM Army Research Laboratory

REPORT DOCUMENTATION PAGE

1. REPORT DATE	2. REPORT TYPE	3. DATES COVERED	
		START DATE	END DATE
December 2025	Technical Report	2024 October 1	2025 September 30

4. TITLE AND SUBTITLE
Modeling the Thermal History–Microstructure Links in Equal Channel Angular Extrusion

5a. CONTRACT NUMBER	5b. GRANT NUMBER	5c. PROGRAM ELEMENT NUMBER
5d. PROJECT NUMBER	**5e. TASK NUMBER**	**5f. WORK UNIT NUMBER**

6. AUTHOR(S)
Philip E. Goins and Kristopher A. Darling

7. PERFORMING ORGANIZATION NAME(S) AND ADDRESS(ES)	8. PERFORMING ORGANIZATION REPORT NUMBER
DEVCOM Army Research Laboratory ATTN: FCDD-RLA-MF Aberdeen Proving Ground, MD 21005	ARL-TR-10244

9. SPONSORING/MONITORING AGENCY NAME(S) AND ADDRESS(ES)	10. SPONSOR/MONITOR'S ACRONYM(S)	11. SPONSOR/MONITOR'S REPORT NUMBER(S)

12. DISTRIBUTION/AVAILABILITY STATEMENT
DISTRIBUTION STATEMENT A. Approved for public release: distribution unlimited.

13. SUPPLEMENTARY NOTES
ORCID: Philip E. Goins, 0009-0005-5135-1200

14. ABSTRACT
The development of cutting-edge materials requires ever more precise control of processing conditions to obtain windows of optimal performance, especially controlling temperature and pressure where islands of performance can be very narrow and sensitive to fluctuations or error, particularly in larger specimens produced by methods under extreme conditions. Detailed awareness of the precise conditions of operations is necessary, especially when attempting to engineer microstructure in complex alloys. In this work, a microstructure model is coupled to a process model that captures the heat transport in the emerging processing approach of equal channel angular extrusion (ECAE), which is a process of severe plastic deformation under shear that is often performed with samples preheated to high temperatures. The precise thermal history may deviate significantly from idealized conditions as heat is lost in contact with the ECAE system and is also generated at points by plastic strain, and that deviation will lead to error in engineering materials for optimal performance, especially during scale-up efforts. This thermal history model is coupled with a microstructure model based on ferrous systems to highlight the coupling of models and create a holistic approach to precisely engineer materials in alignment with current and future experimental and data-driven efforts.

15. SUBJECT TERMS
Sciences of Extreme Materials, Integrated Computational Materials Engineering, Microstructure Evolution, Computational Material Science, Metallurgy, Mechanical Processing

16. SECURITY CLASSIFICATION OF:			17. LIMITATION OF ABSTRACT	18. NUMBER OF PAGES
a. REPORT	b. ABSTRACT	C. THIS PAGE		
UNCLASSIFIED	UNCLASSIFIED	UNCLASSIFIED	UU	26

19a. NAME OF RESPONSIBLE PERSON	19b. PHONE NUMBER *(Include area code)*
Philip E. Goins	(520) 691-4957

STANDARD FORM 298 (REV. 5/2020)
Prescribed by ANSI Std. Z39.18

Contents

List of Figures

List of Tables

1. Introduction

Microstructure controls the final properties and performance of a material. A well-considered and well-processed microstructure can have high strength, hardness, toughness, corrosion resistance, and so on, as compared to "as-cast" material; ill-considered processing can leave a microstructure full of undesired defects such as voids or pores, or simply be unoptimized for a given application, reducing performance or lifetime of the material.[1] However, most microstructure models used to optimize materials operate on idealized processing conditions such as assumed constant temperature. Real-world processing happens under localized and evolving thermal conditions. Many of the temperature-sensitive terms that change microstructure appear in exponential expressions, such as the nucleation rate R_N of new phases or grains[2]:

$$R_N \propto D(T) e^{\frac{\Delta G^*(T)}{RT}} \tag{1}$$

where D is a temperature-dependent diffusion rate term, ΔG^* is a temperature-dependent critical free energy of nucleation, R is the gas constant, and T is temperature. Similarly, average grain size d (over time t) is also thermally activated and thus grain growth is also a strong function of temperature[3,4]:

$$d(t) = \sqrt{m_0 e^{\frac{-Q}{RT}} t + d_0} \tag{2}$$

where m_0 is a grain boundary interface motion rate prefactor, Q is the activation energy of grain boundary motion, and d_0 is the initial grain structure. These two temperature-sensitive behaviors are modeled in this work, but most other features in a material's chemistry and structure are sensitive to temperature due to activation energies, entropic contributions to free energy, and so on, which govern the formation of phases, defects mobility, rate of diffusion, and other such phenomena. Therefore, connecting real thermal and mechanical history to microstructure evolution is critical to ensuring maximal performance under the expected conditions of realized components.

Even within the same component being fabricated, the thermal history can vary widely based on position. This has become a major challenge in additive manufacturing and similar methods, where as a piece is built up, the thermal transport pathway to the build plate (a primary heat sink) becomes longer and hotter, leading to varied and extreme thermal gradients as a component is built.[5–7] While additive manufacturing is given considerable attention from this thermal perspective because of the extremity of thermal inhomogeneity, many older processing models are comparatively less attended to, even as awareness of its

import is known. As thermal history within a component depends on the precise sample geometry as well as processing equipment, a full model must in some sense be prepared for each device (or class of device).

For instance, less attention has been paid to modeling the thermal profiles in other mechanical approaches, including equal channel angular extrusion/pressing (ECAE/ECAP). ECAE is a severe plastic deformation method in which a billet is subjected to intense simple shear by pressing it through two channels of equal cross section intersecting at an angle, most commonly 90° in an L-shaped channel. Unlike conventional extrusion, the billet retains its original cross section, allowing repeated deformation without the need for additional dies. The process can be systematically varied through processing routes, defined by the billet's reorientation between passes. The three standard routes are no rotation, 180° rotation between passes, and 90° rotation between passes. Variant and hybrid routes also exist but are less widely adopted due to geometrically increasing complexity with degrees of freedom and poor predictability, which is a challenging design space that detailed modeling may enable exploration of.

Each pass through a 90° die imposes an equivalent strain of approximately 1.16, comparable to approximately 69% reduction in area under conventional deformation. The shear is concentrated near approximately 45° to the channel intersection, generating high dislocation densities and subdividing grains into progressively refined domains. With successive passes, the shear texture intensifies; unless reversed, a strong crystallographic texture develops. The 180° and 90° rotation mitigates this and encourages a somewhat more equiaxed structure.

Microstructural evolution under ECAE is governed by dislocation accumulation, dynamic recovery, recrystallization, and grain growth, with the degree of refinement and texture intensity controlled primarily by the number of passes and the processing route. The resulting ultrafine-grained microstructures exhibit enhanced strength and hardness, often accompanied by reduced ductility; however, careful route selection and processing optimization can preserve toughness through control of final microstructure with careful tuning of experimental parameters.

Some macro-scale efforts to model mechanical strain and to an extent temperature profile have been made in a more mechanical engineering sense. There are multiple studies mapping the strain fields found in ECAE samples and experimentally measuring the resultant deformed textures in the regime where mechanical influences are dominant, including a detailed look at the plastic deformation zone (PDZ) at the bend in channels.[8–17] A few studies couple temperature with mechanical process, often using constitutive hardening laws and relaxation formulas to couple into a macro thermomechanical system. Most use commercial

software such as Deform-3D or Ansys. Some studies that look at component history as a function of position experimentally measure sample local hardness or grain size and texture as a function of position to motivate the importance of such thermomechanical modeling ex post facto, but do not generally offer the ability to model or predict microstructure or properties beyond semi-empirical relationship fits for a narrow experimental space. The closest realization of a fully linked microstructure model to thermomechanical history is the use of a 2D cellular automata model along with the mechanical history with a simple model for thermal history.[17] Even this approach offered valuable insights and highlights the essentiality of connecting real-world experimental parameters to guide the modeling of microstructure. Ultimately, better linking the entire localized thermomechanical history to resultant microstructure will be necessary in using the technique for fully realized microstructure engineering required for next-generation materials. Further, an additional layer of complexity is necessary when handling hollow billets that serve as cannisters for contained powdered material set to be consolidated, a recent approach for mechanically processing new materials from powders or similar or consider functionally graded or other heterogeneous material. This contrasts nearly every previous effort that examined conventional solid homogeneous billets.[18,19] As consolidation through severe deformation and functional graded materials for optimized performance are both areas of significant ongoing research, capturing them in processing models will be highly valuable.

Here, a thermal history model of the ECAE system is prepared, reflecting the system used presently, using heterogeneous heat transport, and linked to microstructure evolution simulations. The model considers a sample billet that contains a solid exterior and either solid or powder material in a channel in the center (or other heterogeneously arranged material as defined by the user). As the sample enters at a user-defined preheated temperature, contact with the ECAE channel, compaction of the billet core material (increasing density and thermal conductivity, typically), heat generation from plastic work in the PDZ, and so on will cause changes to the thermal profile during each sample pass-through. This model is linked to an explicit volume-based microstructure evolution model, the coupling of which is critical for realistic prediction of microstructure features. This attention to detail will become especially important as data-based models that study materials are increasingly employed. Without accounting, these sources of error could lead to signals that may be misinterpreted by data-driven models, which are sensitive meta system information when comparing results produced from different systems, and paves the way for material specific thermomechanical modeling of materials produced through this important approach, highlighting the importance of fully understanding the systems with which materials are prepared if optimizing results in an agile way is to be realized.

In this work, a thermal model tuned to a real-world system, the custom-built ECAE press system at the U.S. Army Combat Capabilities Development Command (DEVCOM) Army Research Laboratory (ARL) (Figure 1), is used in numerous ongoing metallurgy design and engineering research programs. The thermal model will provide guidance by translating experimental settings to spatial thermal history and coupled to microstructure models, it will provide a crucial link between processing and performance that cannot be neglected. It is likely that the spatial sensitivity in consolidated powdered material and functionally graded material will continue to be an active area of research. Thus, the development of a flexible and easily referenced model is necessary.

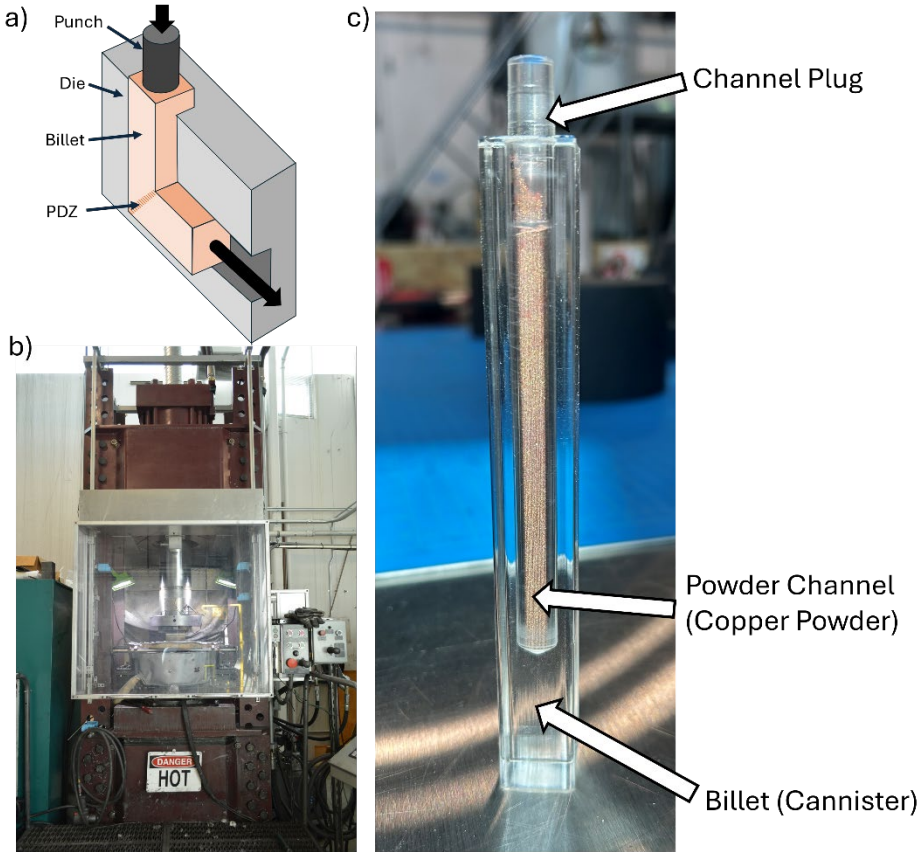

Figure 1. a) A schematic of a general ECAE system. b) A photograph of the custom ECAE system modeled here. c) A transparent prototype of the hollow billet containing a powder channel for consolidation (actual billets are metal).

2. Methodology

The heterogeneous thermal model here uses a pair of cubic Eulerian grids, and computes the thermal transport using the nonhomogeneous heat equation:

$$c_P(x)\rho(x)\frac{\partial T}{\partial t} = \nabla \cdot k(x)(\nabla T) + Q(x) \tag{3}$$

where c_P is the heat capacity, ρ is the density, T is the temperature, k is the thermal conductivity, and Q is any additional heat terms. In this work, Q is primarily the heat generated in the PDZ zone from strain. In the future, a friction term will likely be added in forthcoming versions as the work of DeLo and Semiatin suggests its importance at higher pass rates.[12,14] Any chemical or phase changes, the heat released from sudden microstructure recovery, or radiative loss at surfaces are also readily incorporated as needed but not considered in these examples.

The first grid is for the material billet, for which a user specifies the length, width, height, as well as channel length and channel diameter for the internal cavity for holding the material of interest. The billet cannister itself makes up the remainder of the sample. The user specifies the thermal transport properties of both the bulk contained and cannister materials, as well as some description of the powder conductivity or estimate thereof.

The second grid represents the extruder channel, which is composed of tool steel in this case, though other ECAE systems may use tungsten carbide, which is straightforwardly adjusted in the code header. The ECAE grid is shaped to be a hollow rectangular prism with an internal void of the same cross section of the billet that will pass through it. The boundary conditions of the outside of the extruder are held at a fixed temperature; ECAE systems as this one may have a thermostat with a moderately elevated temperature hold range. The front and back of the extruder are assumed both to be free surfaces and to have negligible heat loss compared to conduction into the thermostat, assumptions that may be relaxed in future versions for high-temperature materials where radiative or convective cooling in air are significant or where the punch contact is also considered. Modeling the ECAE channel surfaces is important because the sample is frequently entered much hotter than the thermostat temperature, so the back of the sample may experience a hotter channel surface than the front of the sample.

The boundary conditions of the billet and the interior channel surfaces are either assumed to be in contact with each other or with air depending on the position of the billet in the channel. In the system, the billet is passed through the extruder and travels at a user-specified rate (here, 1 inch per second, a typically used value). The position of each point of the ECAE system is computed as a function of time with

respect to the billet's position to determine where contact between the two occurs. If two faces in the grid are in partial contact, conduction happens proportionally to the fraction of areal contact. A contact efficiency term is used to modify the rate of transport. While the high pressure of the system should ensure good contact, it is common to apply lubricant between the ECAE system and the billet, which can reduce the rate of thermal transport depending on the lubricant choice and amount. In addition to specifying the rate of movement, it is common to make multiple passes through the ECAE system, which this model also conducts. It is common that the turnaround for these passes is very short, and here we assume they happen in quick succession, but if there is significant lag between passes, modification to billet temperature may also be important to integrate into the model before the pass starts.

As the sample passes through the channel, it will encounter the PDZ (in this system, 60% through the 15-inch channel), which strains the material by a factor of 1.16. We do not account for the local strain's distortion grid geometry currently (which is a studied problem and will be added in future versions as needed), but we do add the thermal energy from shear strain, using the Taylor–Quinney[20] equation:

$$\beta_{TC} \int_0^d W_p = \rho c_P \Delta T \tag{4}$$

where W_p is the plastic work done through work displacement d and β_{TC} is the Taylor–Quinney coefficient, which describes the fraction conversion of plastic work to heat. Generally, values of 0.9 or 0.91 are assumed for the Taylor–Quinney coefficient (though detailed experiments can find deviations in certain loading modes[21]). Thus, as the material passes through the location of the PDZ L-bend, heat from strain is effectively added into the system locally. Further, using user-specified estimates of consolidation, guided by experimental fits or theory, the thermal transport properties of the channel material may be modified as consolidation occurs, typically through increased density and a very sharp jump in thermal conductivity as porous media such as powder is pressed into solid material as consolidation converts packed powder into dense material.[18,19] Additionally, a stored energy term from increased dislocation/defect density can also be passed into the microstructure-level models as well.

Table 1 shows example properties and configuration settings with descriptions used in the examples.

Table 1. Thermal ECAE model parameters.

Property	Value	Description
c_P Billet	392.5 J/(K kg)	Heat capacity of the billet cannister
ρ Billet	8900 kg/m^3	Density of the billet cannister
K Billet	400 J/(m s K)	Thermal conductivity of the billet cannister
L Billet	0.1524 m	Length of the billet
W Billet	0.0254 m	Width and height of the billet
c_P Channel	446.6 J/(K kg)	Bulk heat capacity of the channel material
ρ_{Bulk} Channel	7900 kg/m^3	Bulk solid density of the channel material
$\rho_{Packing}$	0.66	Packing density of the channel material
K Channel (Initial)	5 J/(m s K)	Heat capacity of channel material before pressing
K Channel (Dense)	50 J/(m s K)	Heat capacity of fully dense channel material
L Channel	0.10 16 m	Length of the channel internal to the billet
R Channel	0.003 m	Radius of the channel internal to the billet
c_P Extruder	400 J/(K kg)	Heat capacity of the extruder system walls
ρ Extruder	15,600 kg/m^3	Density of the extruder system walls
K Extruder	200 J/(m s K)	Thermal conductivity of the extruder system walls
L Extruder	0.381 m	Length of the extruder system passage
T Extruder	0.0254 m	Thickness of the extruder system passage walls
k Contact	0.025	Contact efficiency between extruder and billet
ε L-Bend	1.16	Strain applied at L-bend
Y_f	200 MPa	Flow stress of the billet
L Strain Zone	0.005 m	Effective width of the applied strain area
β	0.91	Taylor–Quinney (strain to thermal) conversion ratio
v Billet	0.0254 m/s	Velocity of billet through the extruder system
T Billet	1000 °C	Initial billet temperature
T Extruder	400 °C	Extruder system thermostat temperature

Properties were taken from real-world materials tested in processing copper and iron for the billet and cannister material, respectively, and tungsten carbide for the ECAE system channel material. Heat capacities were assumed to be 3R in terms of joules per mole kelvin.

3. Results and Discussion

An example thermal heat map of the flow of this material through the ECAP extruder is shown in a cutaway in Figure 2. As can be seen, the sample cools rapidly in contact with the much colder surface, but as the extruder channel itself heats up from contact with the hot sample, the back end of the billet may cool more slowly as it passes than the front end. A diagonal band of increased temperature is visible in the 50% and 66% periods shown; this is heat being generated as the sample passes through the PDZ.

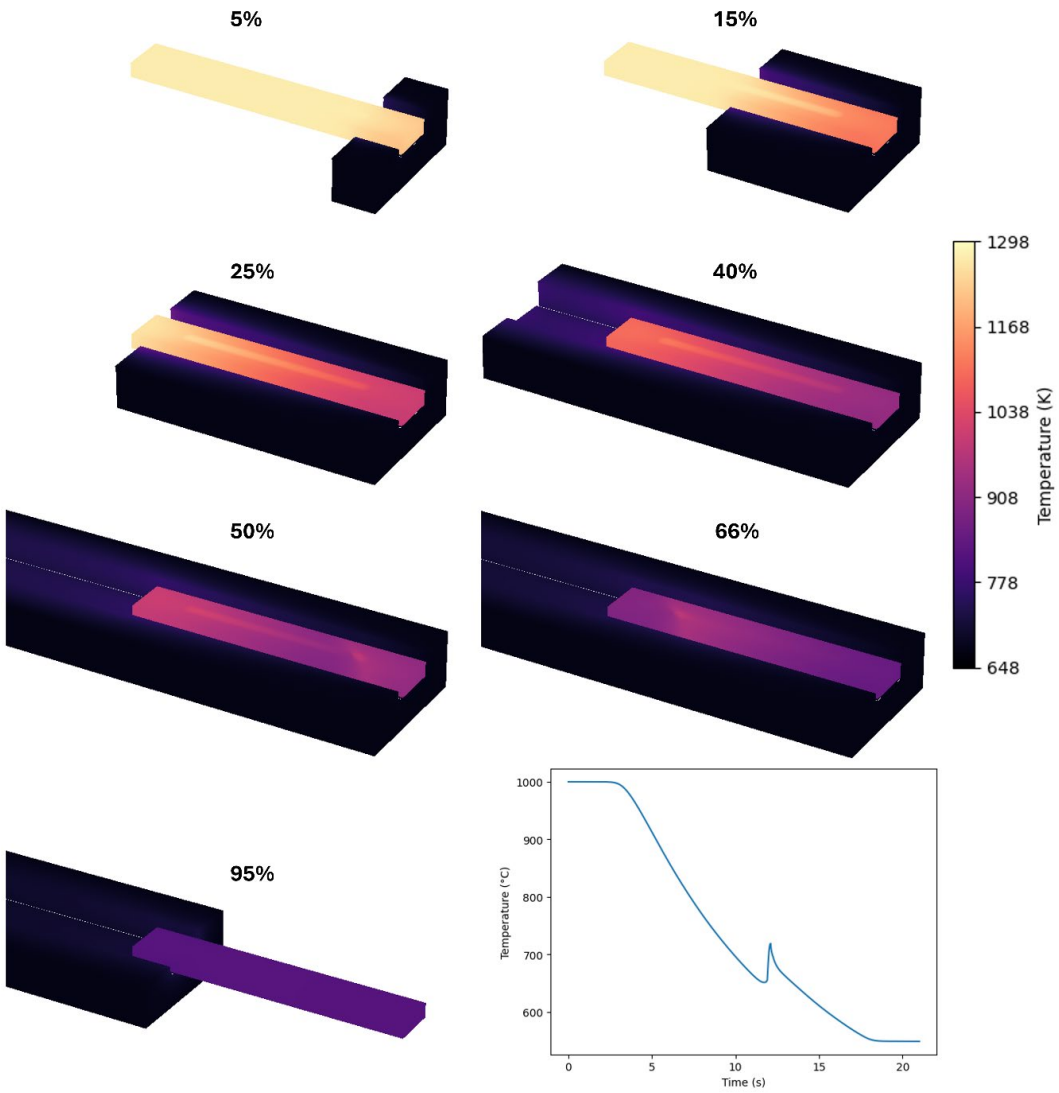

Figure 2. A map of temperature cutaway as a percentage of time passed through the ECAE channel, with a starting temperature of 1000 °C, for a single pass. An inset shows the temperature profile over time for the sample center.

A plot of the predicted temperature at the front of the canned channel material (first to enter the extruder) is shown in Figure 3a, and the temperature difference between the front of the cannister and back of the cannister as a function of position in the extruder system (rather than time) is shown in Figure 3b. The temperature difference between front and back of cannister material for a given position within the ECAE system is comparatively small, with a spread of a few degrees with the parameters shown here when tested running typical system settings. A spread of approximately 5–10 °C, which is typically observed depending on parameters tested, could be significant if the material is near a phase transformation or other critical temperature. Nucleation rates and other activations are famously sensitive to temperature around certain temperature thresholds. For other systems,

approximately 5–10 °C may be relatively insignificant, and the spatial component of thermal history can safely be ignored. Importantly, both the front and back of the channel, if contact is strong between the extruder and billet, a temperature decrease is predicted around nearly 200 °C by the time the PDZ is reached, which is a very significant amount of thermal loss for most purposes in systems at 1000 °C, such as the hot billets simulated here. Further, the plots above are aligned based on position, but the back of the channel spends much longer at high temperature than the front in terms of time. If the thermal history before passing the L-channel at all impacts the final microstructure, this too will have an impact on the final microstructure. Similarly, the front of the channel will spend much longer at higher temperatures *after* passing the PDZ, as the billet cannot be quenched or otherwise quickly brought to room temperature until the entire piece has fully cleared the ECAE channel and is removed.

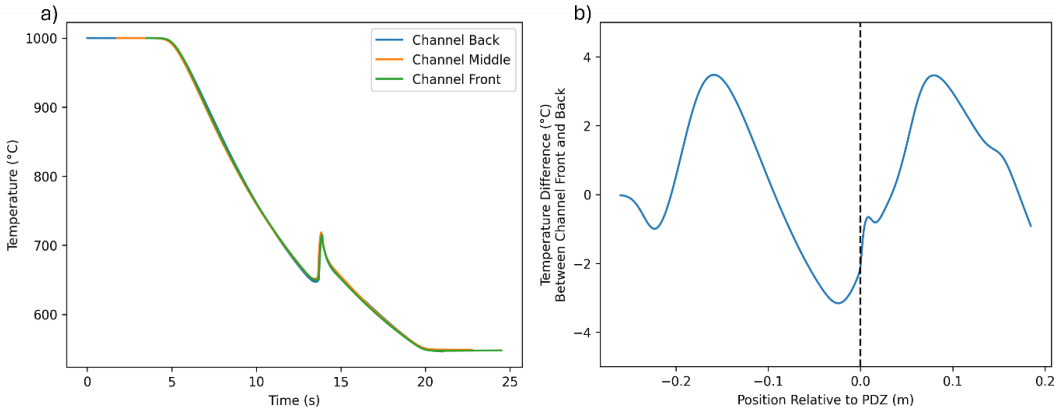

Figure 3. a) Thermal history of the canistered material in the billet channel at different points, realigned based on position through the ECAE system, with an initial sample temperature of 1000 °C. b) Difference between the front and back of the powder channel for a given position in the ECAE system (zeroed around the PDZ). The temperature difference between the two positions in the billet powder channel tended to be around ±5 °C at most in many settings.

Conversely, if a cold (room temperature) sample was passed in, a temperature rise in the PDZ of around 90 °C would be expected, which may matter for some lower-temperature systems (and also may be too hot to handle unaided), as shown in Figure 4, which presents an example run where the ECAE and billet both start at room temperature and the sample reaches above 120 °C before cooling down to a bit over 60 °C when exiting the channel. In this case, weaker contact assumptions would result in a higher final temperature on exit, and modest but appreciable differences do exist in the thermal history along the channel in the billet. For materials that are very nonequilibrium, such as nonstabilized nanocrystalline materials, even modest temperature rises can engender appreciable microstructure evolution.

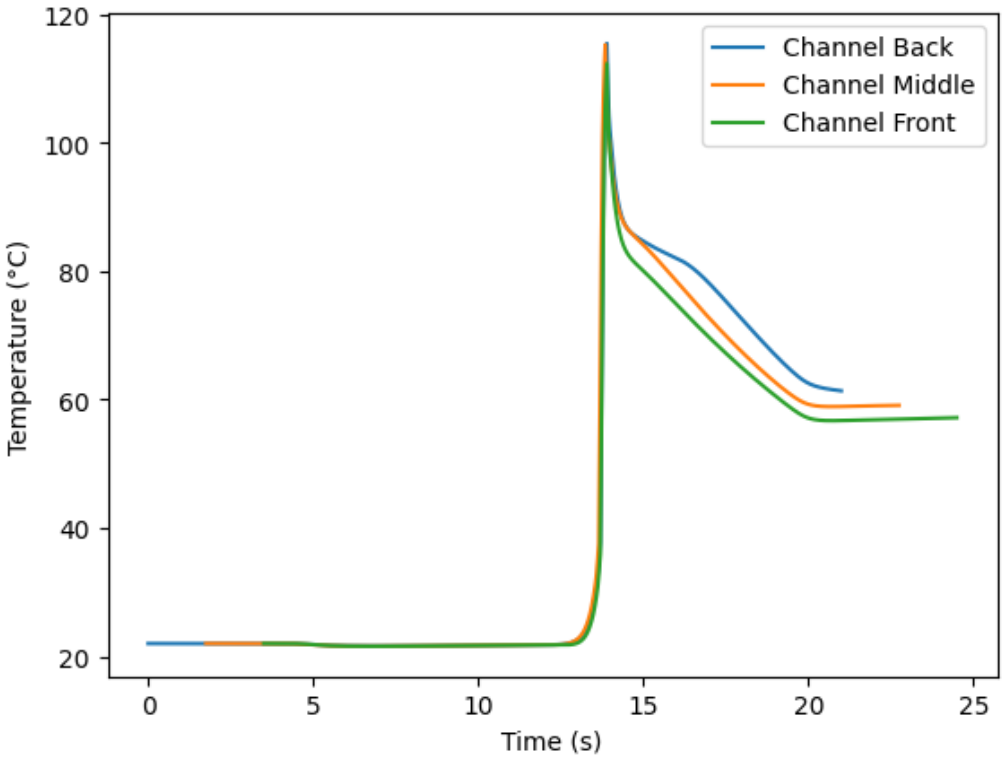

Figure 4. Thermal history of the front, center, and back of the powder channel inside the billet material, realigned based on position through the ECAE system, where the initial ECAE thermostat and sample are passed through at room temperature. While similar, each part of the powder channel does experience a somewhat unique thermal history as it passes through the ECAE system even if the only source of heat is that generated from the mechanical deformation of the billet in the PDZ.

As discussed, the central thrust of this work is to link microstructure to thermal histories, and to demonstrate this capability, an illustrative microstructure evolution model is shown here, using an extended and partially parameterized Monte Carlo Potts model for grain growth and recrystallization.[22] An initial microstructure is seeded by straining a structure generated by ideal grain growth for 300 Monte Carlo steps with dimensions of 128 × 128 × 256 voxels (which are parameterized at 1 μm per voxel), which is then compressed into 128^3 to create an initial elongated grain structure instantiation. This initial microstructure is thus comprised of reasonably large grains that have been compressed with a strain of approximately 1, which is a simple way of instantiating a microstructure that has undergone heat treatment and subsequent deformation. In typical settings, billets are often heat-treated in a furnace for some time before ECAE processing; the initial microstructure chosen should naturally reflect the starting state of any materials being studied. This initial microstructure is passed into the more realistic recrystallization and grain growth model using a chosen temperature–time profile loaded from the thermal model. The extended Monte Carlo Potts model here assumes a volume of material with a given

grain and phase state at each site on a grid, and sites are randomly selected for proposed updates from grain/phase state *i* to grain/phase state *j*, with a success probability for update of

$$p_{ij} = \begin{cases} M_{ij} & \Delta E_{ij} \leq 0 \\ M_{ij}\gamma_{ij} e^{\Delta E_{ij}/kT} & \Delta E_{ij} > 0 \end{cases} \quad (5)$$

Here, ΔE_{ij} is the energy change from state *i* to *j*, M_{ij} is the interfacial mobility between grains/phases *i* and *j*, $\boldsymbol{\gamma_{ij}}$ is the interfacial energy between *i* and *j*. The kT term here is a simulation temperature that is not generally set to physical values for grain growth. A value around 0.5–2.0 is typically used for grain growth to avoid some artifacts due to the grid symmetry. The energy and mobility functions are given below in the following equations:

$$\Delta E_{ik} = \sum_{k=0}^{26} (\delta_{ik} \cdot \gamma_{ik}) + \Delta\eta_{ik} \quad (6)$$

Here, δ_{ij} is the Kronecker delta between states *i* and *k*, $\boldsymbol{\gamma_{ij}}$ is the interfacial energy between the states *i* and the state found at site *k*, and $\Delta\eta_{ij}$ is the volumetric energy difference (for the volume of a single site) between states *i* and *k*, in this case driven by stored plastic strain energy in the material. In short, the interfacial energy is dictated by the number of unlike nearest neighbors of the 26 neighboring cells (in a 3 × 3 × 3 compact stencil around the center) and the bulk energy values of each state. The interfacial energy itself is dictated by a Read–Shockley type relationship to incorporate anisotropy effects,[23] and the mobility is scaled with an activation energy against physical temperature with a prefactor dictated by the maximum temperature but otherwise is unparameterized in this work.

$$\gamma_{ij}(\theta_{ij}) = \begin{cases} \gamma_{max} & \theta \geq 15° \\ \gamma_{max}\left(\theta/\theta_{max}\right)\left(1 - \ln \theta/\theta_{max}\right) & \theta < 15° \end{cases} \quad (7)$$

$$M_{ij} = M_0 e^{Q_B/RT} \quad (8)$$

Here, *Q* is taken to be 60 kJ**,** which is a typical self-diffusion value for iron.[24] In all cases, grain boundary energy and mobility follow a Read–Shockley type formalism, with all grains existing at the start holding about 10 J/mol stored energy, which is similar to or lower than comparably strained material.[25] Nucleation of strain-free grains is permitted using classical nucleation theory. Simulations are carried out on 128^3 grids, where each voxel edge length is uniform at 1 μm (for the purposes of unitizing energy per area and energy per volume). Units of time (i.e., boundary mobility and nucleation rate) are only approximately parameterized in this work. Three illustrative cases are shown in this report: one using the thermal history of the front position of the billet channel, one using the back position of the billet channel, and one using the naive temperature assumed at the start of the run,

which is likely the value a model would use absent more realistic thermal history, at the center of the billet channel. All three cases start time immediately after passing through the PDZ (where a powder material would experience extreme strain and be consolidated) and terminate time either when the entire billet has passed through the channel (and would be rapidly cooled off) or when grains grow so large that self-impingement across the periodic boundaries is imminent (i.e., the grains have become too large to be properly contained in the simulation window), past which simulation results become unphysical and invalid.

As shown in Figure 5, there is a significant difference between the final microstructure from an idealized constant 1000 °C as simulated versus including the thermal history profile under these conditions. While the material constants chosen are for this example somewhat unparameterized, the temperatures and activation energies chosen are representative of those found in real ferrous systems (and are the subject of ongoing work using the ECAP thermal model developed here). It is expected that understanding the actual experienced thermal history of materials is necessary to properly engineer optimal performing materials through selection of processing parameters; this is especially critical in linking small-scale laboratory components to larger-scale materials production where size dependence will strongly impact actual experienced thermal histories in processing. Similarly, within each component, the thermal history can also vary somewhat in a way that can be significant.

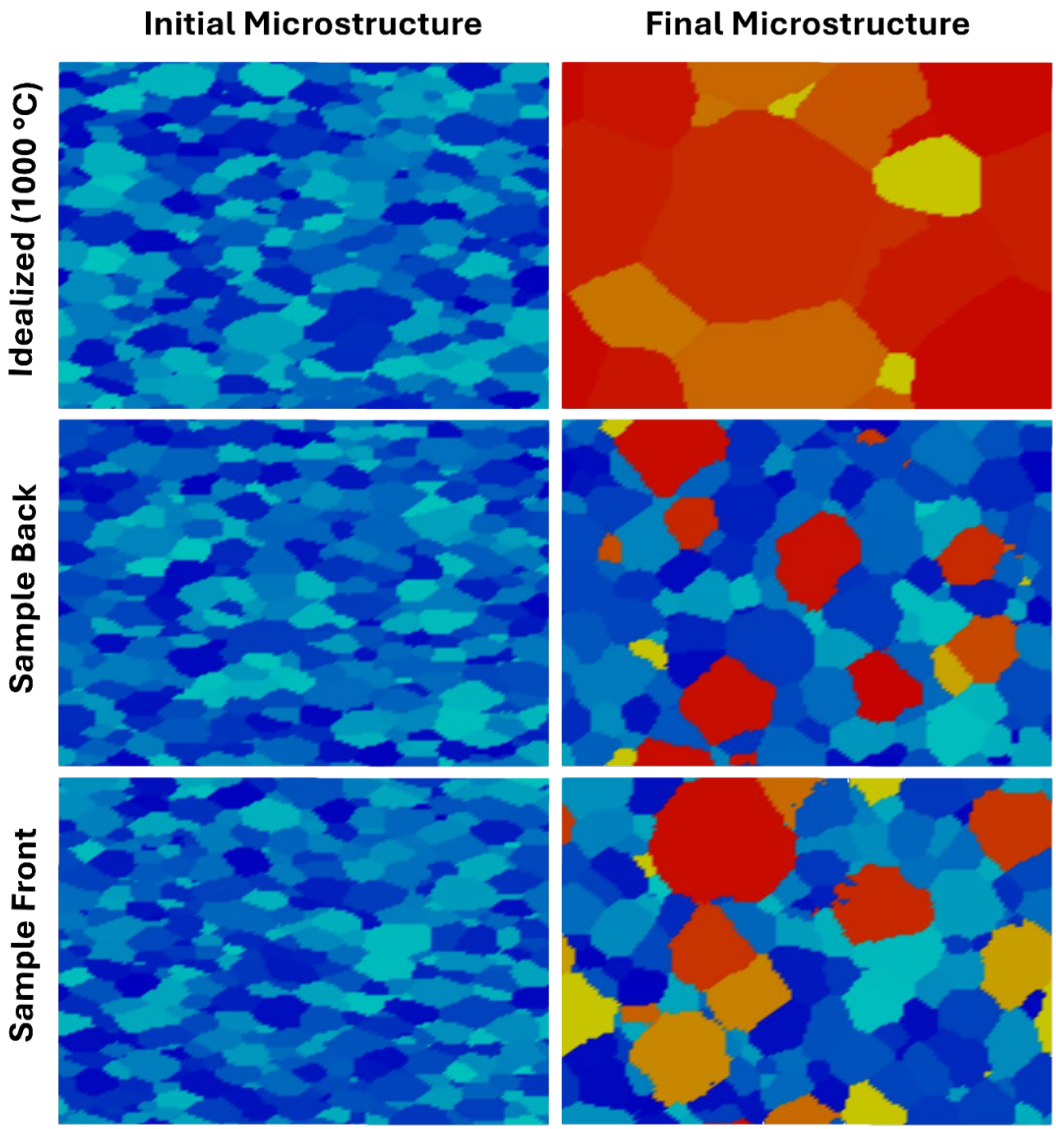

Figure 5. Microstructure model of grain growth and recrystallization for the idealized 1000 °C case, using the simulated thermal history of the billet cannister back and front for the example settings selected. Blue grain hues indicate grains from the original microstructure, and red through yellow hues are nucleated recrystallized grains.

The naïve assumption of a constant 1000 °C sees a 100% complete recrystallization and very large grain size (as the only remaining grains are large, recrystallized grains). In fact, these simulations *understate* the grain size difference as they were terminated early to avoid self-impingement across the periodic boundary condition (due to large grain size relative to simulated volume). For the same microstructural parameters (activation energies and kinetics terms fixed under an Arrhenius relationship assumption), the resultant microstructure from predicted thermal history was very different. Both were still in the process of undergoing recrystallization at the termination of the processing, rather than achieving complete recrystallization. A slightly higher temperature during the early stages of

nucleation resulted in an initially faster recrystallization rate at the back of the sample's canister channel. However, because the front of the sample experiences longer periods at high temperatures after the PDZ in the channel, the front end achieves higher final recrystallization end state, about 31% recrystallized compared to 15% for the sample back (Figure 6). Grain size follows a similar trend, with modest differences along the position within a simulated ECAE sample, and very different results from the idealized non-simulated assumptions. Most of the reason for the substantial difference in mean grain size is because in the "ideal" case, all grains are fully recrystallized grains, while many small grains remain in the cases that use predicted thermal histories that keep the mean grain radius much smaller. While the sample temperature was taken to be one that is expected to be in a particularly sensitive region in the material response, all activation energies and temperatures selected are realistic for materials and experimental conditions used in current research efforts. Iron remains a relatively important alloy base element in metallurgy. At minimum, this demonstrates it is important to be aware of the real experienced thermal conditions of a sample, rather than relying on idealized assumptions when control of microstructure is required to optimize material properties and performance. Further, this approach offers hope for much more sophisticated microstructure engineering from ECAE (and similarly) processed materials, which will be necessary to design the next generation of cutting-edge performant materials.

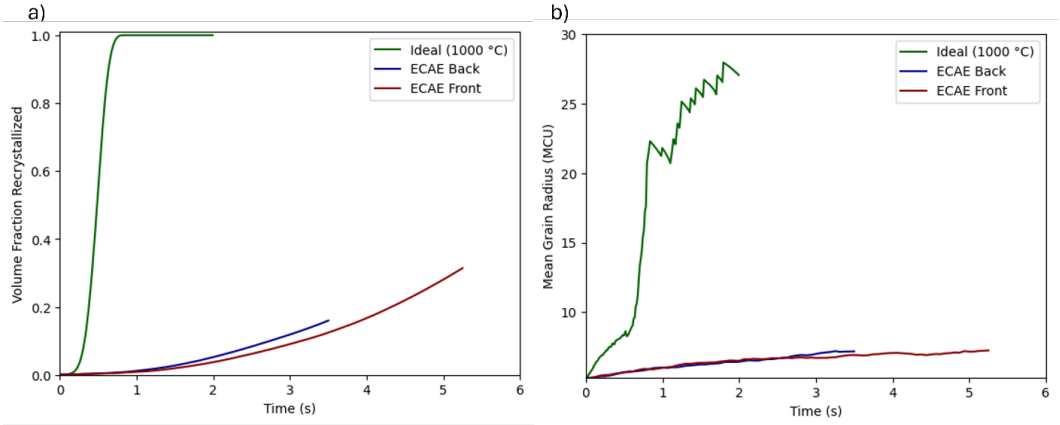

Figure 6. a) Recrystallization fraction as a function of time following the pass through the ECAE PDZ for the idealized 1000 °C as well as the simulated thermal histories, and b) the mean grain size as a function of time following the pass through the ECAE PDZ for the idealized 1000 °C as well as the simulated thermal histories.

As for the recrystallization timescale, while recrystallization occurring within 1 s may appear rapid, this is consistent with literature suggesting recrystallization in iron happens on the timescale of less than a second to a few seconds around 1000 °C, while those timescales extended to tens of seconds to minutes for full

recrystallization for isothermal treatments of 800–900 °C, depending on alloy, strain degree, and other conditions.[26–28] Most iron/steel recrystallization studies are done at lower temperatures to achieve a more granular temperature–time study, but the temperature ranges simulated here are reflective of temperatures commonly performed in the actual ECAE processing of hot billets.[29] Considering this model is only loosely parameterized particularly for kinetics, the agreement with real-world timescales here is surprisingly good, underscoring the difference between the assumed temperature and the actual temperature could have significant impact on the final microstructure. The ability to couple microstructure and detailed thermal history will enable more precise microstructure engineering and deepen system understanding when trying to process results from ECAE experiments. It is hoped the value of this approach will be increased as integration of computational materials design and engineering continues, leveraging these capabilities in a wider workflow.

4. Conclusions

Here, a thermal transport model of a heterogeneous-material ECAE system linked to 3D microstructure evolution has been constructed. The application is to better understand the potential impacts of thermal and material inhomogeneity that naturally occur in ECAE, especially when studying heterogeneous systems or consolidation of powders in channeled billets. Even modest differences in temperature from idealized conditions are shown to potentially matter significantly in the evolution of the microstructure in systems with thermally activated behaviors, and capturing accurately is critical in many materials currently studied. Expanding on this model, such as by linking a more-detailed, dedicated mechanical model, readily found in literature, will result in a more accurate model for engineering real materials in the future. Further, this model will provide useful features in wider integration into computational materials engineering workflows, especially as it becomes applied to inhomogeneous and structured materials.

5. References

1. DeHoff RT. Engineering of microstructures. Mater Res. 1999;2(3). https://doi.org/10.1590/S1516-14391999000300002
2. Karthika S, Radhakrishnan TK, Kalaichelvi P. A review of classical and nonclassical nucleation theories. Crys Growth Des. 2016;16(11):6663–6681. https://doi.org/10.1021/acs.cgd.6b00794
3. Mullins WW. Two-dimensional motion of idealized grain boundaries. J Appl Phys. 1956;27:900–904. https://doi.org/10.1063/1.1722511
4. von Neumann J. Metal interfaces. Am Soc Met. 1952:108–110.
5. Tan JHK, Sing LS, Yeong WY. Microstructure modeling for metallic additive manufacturing: a review. Virtual Phys Prototyp. 2020;15(1):87–105. https://doi.org/10.1080/17452759.2019.1677345
6. Gatsos T, Elsayed KA, Zhai Y, Lados DA. Review on computational modeling of process–microstructure–property relationships in metal additive manufacturing. JOM. 2020;72:403–419. https://doi.org/10.1007/s11837-019-03913-x
7. Körner C, Markl M, Koepf JA. Modeling and simulation of microstructure evolution for additive manufacturing of metals: a critical review. Metall Mater Trans A. 2020;51(10):4970–4983. https://doi.org/10.1007/s11661-020-05946-3
8. Djavanroodi F, Omranpour B, Ebrahimi M, Sedighi M. Designing of ECAP parameters based on strain distribution uniformity. Prog Nat Sci Mater Int. 2012;22(5):452–460. https://doi.org/10.1016/j.pnsc.2012.08.001
9. Cui HJ, Goforth RE, Hartwig KT. The three-dimensional simulation of flow pattern in equal-channel angular extrusion. JOM. 1998;50(8).
10. Gholinia A, Prangnell PB, Markushev MV. The effect of strain path on the development of deformation structures in severely deformed aluminium alloys processed by ECAE. Acta Mater. 2000;48(5):1115–1130. https://doi.org/10.1016/S1359-6454(99)00388-2
11. Chung SW, Kim W-J, Kohzu M, Higashi K. The effect of ram speed on mechanical and thermal properties in ECAE process simulation. Mater Trans. 2003;44(5):973–980. https://doi.org/10.2320/matertrans.44.973

12. DeLo DP, Semiatin SL. Finite-element modeling of nonisothermal equal-channel angular extrusion. Met Mater Trans A. 1999;30:1391–1402. https://doi.org/10.1007/s11661-999-0287-2

13. Pei Q-X, Lu C, Fu MW. Coupled thermo-mechanical analysis of severe plastic deformation for producing bulk nanostructured materials. Adv Eng Mater. 2004;6(12):933–936. https://doi.org/10.1002/adem.200400100

14. Purnowidodo A, Aminnudin A, Irawan YS. The analysis of friction effect on equal channel angular pressing (ECAP) process on aluminium 5052 to homogeneity of strain distribution. East Eur J Ent Tech. 2022;92(2):72. https://doi.org/10.15587/1729-4061.2018.127006

15. Al-Alimi S et al. Effects of preheating temperature on deformed AA6061 aluminium properties of equal channel angular pressing (ECAP) by using Deform-3D software. Arab J Sci Eng. 2023;48:3381–3389. https://doi.org/10.1007/s13369-022-07149-x

16. Alateyah AI et al. Effect of ECAP die angle on the strain homogeneity, microstructural evolution, crystallographic texture and mechanical properties of pure magnesium: numerical simulation and experimental approach. J Mater Res Tech. 2022;17:1491–1511. https://doi.org/10.1016/j.jmrt.2022.01.088

17. Gzyl MZ, Rosochowski A, Milenin A, Olejnik L. Modelling microstructure evolution during equal channel angular processing of magnesium alloys using cellular automata finite element method. Comp Meth Mater Sci. 2013;13(2):357–363. https://doi.org/10.7494/cmms.2013.2.0454

18. Darling KA et al. Microstructure and mechanical properties of bulk nanostructured Cu–Ta alloys consolidated by equal channel angular extrusion. Acta Mater. 2014;76:168–185. https://doi.org/10.1016/j.actamat.2014.04.074

19. Levin ZS, Wang X, Kaynak M, Karaman I, Hardwig KT. Strength and ductility of powder consolidated ultrafine-grain tantalum. Int J Refract Met Hard Mater. 2019;80:73–84. https://doi.org/10.1016/j.ijrmhm.2018.12.017

20. Taylor GI, Quinney H. The latent energy remaining in a metal after cold working. Proc Royal Soc A. 1934;143(849):307–326. https://doi.org/10.1098/rspa.1934.0004

21. Rittel D, Zhang LH, Osovski S. The dependence of the Taylor–Quinney coefficient on the dynamic loading mode. J Mech Phys Sol. 2017;107:97–114. https://doi.org/10.1016/j.jmps.2017.06.016

22. Grest GS, Anderson MP, Srolovitz DJ. Domain-growth kinetics for the Q-state Potts model in two and three dimensions. Phys Rev B. 1988;38(7):4752–4760. https://doi.org/10.1103/PhysRevB.38.4752

23. Read WT, Shockley W. Dislocation models of crystal grain boundaries. Phys Rev. 1950;78(3):275–289. https://doi.org/10.1103/PhysRev.78.275

24. Buffington FS, Hirano K, Cohen M. Self diffusion in iron. Acta Metal. 1961;9(5);434–439. https://doi.org/10.1016/0001-6160(61)90137-7

25. Sendrowicz A, Myhre AO, Yasikov IS, Vinogradov A. Stored and dissipated energy of plastic deformation revisited from the viewpoint of dislocation kinetics modeling approach. Acta Mater. 2022;237(15):118190. https://doi.org/10.1016/j.actamat.2022.118190

26. Xu X et al. Experimental and theoretical study on static recrystallization of a low-density ferritic steel containing 4 mass% aluminum. Mater Des. 2019;180(15):107925. https://doi.org/10.1016/j.matdes.2019.107924

27. Maeda K, Zhou T, Zurob H. Hot deformation behavior of an Fe–Al alloy steel in the two phase region [thesis]. McMaster University, Department of Materials Science and Engineering; 2014.

28. Yoshie A et al. Effect of dislocation density in an unrecrystallized part of austenite on growth rate of recrystallizing grain. ISIJ Int. 1996;36(4):444–450. https://doi.org/10.2355/isijinternational.36.444

29. Ye W, Gall RL, Saindrenan G. A study of the recrystallization of an IF steel by kinetics models. Mat Sci Eng A. 2002;332(1–2):41–46. https://doi.org/10.1016/S0921-5093(01)01715-4

List of Symbols, Abbreviations, and Acronyms

2D/3D	Two-/Three-Dimensional
ARL	Army Research Laboratory
DEVCOM	U.S. Army Combat Capabilities Development Command
ECAE	Equal Channel Angular Extrusion
ECAP	Equal Channel Angular Pressing
PDZ	Plastic Deformation Zone

1 (PDF)	DEFENSE TECHNICAL INFORMATION CTR DTIC OCA
1 (PDF)	DEVCOM ARL FCDD RLB CI TECH LIB